International Journal of Pharmaceutics 407 (2011) 197–206

Contents lists available at ScienceDirect

International Journal of Pharmaceutics

journal homepage: www.elsevier.com/locate/ijpharm

# Water state effect on drug release from an antibiotic loaded polyurethane matrix containing albumin nanoparticles

Andrea Martinelli*, Lucio D'Ilario, Iolanda Francolini, Antonella Piozzi

*Department of Chemistry, Sapienza University of Rome, P.le A. Moro 5, 00185 Rome, Italy*

ARTICLE INFO

*Article history:*
Received 3 August 2010
Received in revised form 11 January 2011
Accepted 16 January 2011
Available online 21 January 2011

*Keywords:*
Freezing and non freezing water
Nano-composites
Nanoparticles
Drug delivery systems
Albumin
Polyurethanes

ABSTRACT

Water mobility plays a crucial role in determining transport properties of small molecules in polymer matrices. In particular, in drug delivery systems, water state affects the pharmacokinetics, especially drug absorption, diffusion and release. In the present study, the state of water in an antibiotic-loaded composite consisting of albumin nanoparticles ($BSA_{np}$) dispersed into a carboxylated polyurethane (PEUA) has been investigated and compared with that of the single drug-loaded components. The antibiotic cefamandole nafate was used as a model drug. DSC analysis, used to evaluate the freezing and non-freezing water fractions in the hydrated samples, showed that in $BSA_{np}$ water can adsorb both in the inter-particles regions and inside the particles. With increasing of total adsorbed water amount, the contribution of the freezing water fraction was higher than the non-freezing one. As for PEUA, the majority of water molecules absorbed is in a mobile freezing state (about 60% of the $W_{tot}$).

As for the PEUA/$BSA_{np}$ composite, the higher polyurethane phase segregation induced by the nanoparticles as well as the higher non-freezing water fraction significantly enhanced drug uptake with respect to PEUA. Moreover, the greater non-freezing water fraction allowed the drug to penetrate within BSA nanoparticles and to give rise then to a controlled drug release. Indeed, the diffusion barrier exerted by nanoparticles and the matrix prolonged the antimicrobial activity from 4 to 9 days.

Finally, the higher polyurethane phase segregation also improved composite mechanical properties, as evidenced in stress–strain experiments and dynamic mechanical analysis.



## 1. Introduction

Different polymer properties, such as solute permeability and diffusion, mechanical and thermal behaviour, as well as biocompatibility and ability to adsorb and release drug in controlled fashion are strongly influenced by water distribution in the material (Elomaa et al., 2000; Hirata et al., 1999; Rault et al., 1995; Schneider et al., 1993; Tanaka et al., 2002).

Indeed, mobility of water molecules in swollen hydrophilic polymers is tightly related to the interactions they establish with the host matrix and to their geometrical confinement. In general, in relation to the water thermal behaviour, the water state in hydrated materials may be divided into three categories: non-freezing water, freezing bound water and free water (Hatakeyama et al., 1998; Li et al., 2005; Luukkonen et al., 2001). The first kind of water does not crystallize even at high supercooling ($\Delta T_m = 100\,^\circ C$) because of its restricted mobility due to the strong hydrogen bond interactions with the swollen material polar groups. Free water crystallizes in dynamic cooling at low supercooling, up to $\Delta T_c = -10$ to $-13\,^\circ C$. It melts at $0\,^\circ C$ similarly to pure (bulk) water and is related to the liquid molecules not bound to the matrix. Finally, the freezing bound water consists of molecules with an intermediate mobility due to weaker interaction (secondary or tertiary hydratation shell) or because confined in nano-cavity (Faroongsang and Sukonrat, 2008; Ping et al., 2001). It is characterized by a phase transition temperature lower than that of the free water.

In general, the exact definition of the water state may be inferred in chemically and structurally homogeneous systems. Actually, the wide distribution of interaction energies or cavity size, controlling the molecule degrees of freedom, brings about to a more complex behaviour, as evidenced by water crystallization (or ice melting) occurring over a wide temperature range and through multiple, partially overlapping transitions.

As for materials employed in biomedical applications, the early interactions established between the polymer and the water of body fluids influence material biocompatibility, playing a crucial role in the polymer swelling and protein adsorption (Tanaka and Mochizuki, 2004).

Also in controlled drug delivery systems, the adsorbed water state affects the pharmacokinetics, influencing drug solubility, absorption/desorption, diffusion and matrix interaction with the body tissue (Aoki et al., 1995; Katzhendler et al., 2000; Siepmann

* Corresponding author. Tel.: +39 06 49913950; fax: +39 06 490631.
*E-mail address:* andrea.martinelli@uniroma1.it (A. Martinelli).

0378-5173/$ – see front matter © 2011 Elsevier B.V. All rights reserved.
doi:10.1016/j.ijpharm.2011.01.029

and Peppas, 2001). In general, it has been observed that drug transport and release is mainly due to the freezing water into the polymer matrix (Zentner et al., 1979). However, the influence of the adsorbed water state on the kinetics drug release has been so far poorly investigated.

In this study, the state of water adsorbed to a composite matrix, already developed by our group as drug delivery system and based on a carboxylated polyurethane matrix containing albumin nanoparticles (PEUA/$BSA_{np}$) (Crisante et al., 2009) was investigated. Since Crisante et al. showed that the composite, loaded with the antibiotic cefamandole nafate, possessed longer antimicrobial activity with respect to both BSA nanoparticles and PEUA alone, we believe that the knowledge of water interaction with the composite as well as its distribution within the system is important to understanding the different kinetics behaviour exhibited by the single components ($BSA_{np}$ and PEUA) and the composite itself. Further, the results that will be obtained in this study may provide essential information not only for our specific system but also for the design of other types of nanocomposites always aimed to the development of drug controlled release systems.

As for the composite preparation, a segmented polyurethane was chosen due to its good physical and mechanical properties along with a fairly good biocompatibility and antithrombogenicity that make it suitable for application in the biomedical field, including as drug delivery systems (Marconi et al., 1992; Piozzi et al., 2004a).

The presence of highly polar groups in the polyurethane hard segment increases polymer hydrophilicity and allows further modification of material through specific bulk or surface reactions. Different functional groups, introduced in principal or side chain of the segmented polyurethane, have been already exploited by our group to bind bioactive molecules, like heparin (Marconi et al., 1992, 1993), or antibiotics (Piozzi et al., 2004b; Ruggeri et al., 2007) or silver ions (Francolini et al., 2006, 2010). However, it was observed that in these systems only the antibiotic adsorbed on the polymer surface was released. In this regard, the entrapping of BSA nanoparticles in the carboxylated polymer has been shown to be a winning strategy to ensure either an increase in drug adsorption, due to a greater surface/volume ratio, or an improvement in the release of the drug penetrated into the surface underlying layers thanks to enhanced polymer hydrophilicity.

On the other hand, albumin nanoparticles have been already proposed in biomedical application as quantum dot carriers or in formulations for drug sustained release, like anti-cancer molecules, monoclonal antibodies and antiviral (Akasaka et al., 1988; Green et al., 2006; Hanaki et al., 2003; Merodio et al., 2001; Michaelis et al., 2006). The interest in such systems resides in the fact that they are biodegradable, biocompatible, non-antigenic and easy to prepare in a controlled size, distribution and surface composition (Weber et al., 2000).

To evaluate the state of water molecules and their distribution into the hydrated materials, differential scanning calorimetry (DSC) was employed while to verify the effects of the dispersed BSA nanoparticles on the mechanical and viscoelastic polymer properties, stress–strain and dynamic mechanical thermal experiments were carried out.

Finally, according to the obtained results, we tried to explain the role played by the single components in determining the physical and drug release properties of the swollen composite.

## 2. Experimental

### 2.1. Sample preparation

Cross-linked bovine serum albumin nanoparticles ($BSA_{np}$) were prepared by water-in-oil single emulsion as reported in a previous paper (Crisante et al., 2009). Briefly, an aqueous solution of albumin (BSA, Sigma) was added under vigorous stirring to hexane containing sorbitan monoleate (Aldrich) as surfactant. After the emulsion was formed, glutaraldehyde (Fluka) was added as cross-linking agent. The nanoparticles were then separated from the organic phase by centrifugation and purified by soxhlet extraction with isopropanole. Finally, the protein nanospheres were washed in water, where they were finally suspended. The average size of $BSA_{np}$, measured by Laser Diffraction Analyzer, was $430 \pm 10$ nm (Crisante et al., 2009).

The synthesis of the carboxylated polyurethane (PEUA) was carried out by a typical two steps solution polymerization process, by using methylene bis-phenyl-diisocyanate, polypropylene oxide ($M_n = 1200$) as macrodiol and dihydroxymethyl-propionic acid as chain extender in 2:1:1 molar ratio, respectively. The weight-average molecular weight was $M_w = 40{,}000$ as determined by Gel Permeation Chromatography. The detailed synthesis procedure was reported elsewhere (D'Ilario et al., 2002; Marconi et al., 1991). The polymer is not cytotoxic (Crisante et al., 2009) and is structurally similar to other polyurethanes employed for medical devices, including catheters, heart valves and vascular prostheses.

For the composite preparation, the $BSA_{np}$ suspending liquid was changed from water to tetrahydrofuran (THF), by repeated washing and centrifugation steps. Then, a known amount of THF suspended nanoparticles was thoroughly mixed with a PEUA THF solution (30 wt.%). The final weight ratio PEUA:$BSA_{np}$ in the PEUA/$BSA_{np}$ composite was 3:1. About 200 μm thick PEUA and PEUA/$BSA_{np}$ films were prepared by casting the solutions in Teflon circular mould (diameter 10 cm). The films were dried in air at room temperature for 24 h and in vacuum at 70 °C until constant weight.

As far as the procedures for cefamandole nafate (ELI-LILLY, CEF) loading, the study of its kinetics of release and the antimicrobial tests are concerned, they are reported in a previous work by Crisante et al. (2009).

Briefly, to carry out the antibiotic adsorption, either $BSA_{np}$, PEUA or the composite were kept in contact with a 0.04 M antibiotic solution for 24 h at room temperature. When $BSA_{np}$ were employed, they were previously introduced in a SpectaPor cellulose dialysis tube (cut-off of 12,000–14,000 Da). Then, the samples were washed with deionized water for 2 h to remove the un-bonded antibiotic. The amount of adsorbed cefamandole was evaluated by UV–vis spectroscopy at 270 nm, testing the solutions before and after the contact with the samples.

The kinetics of antibiotic release was studied by keeping samples in physiological saline solution for increasing times and determining the eluted drug amount by UV–vis spectroscopy.

The antimicrobial activity of samples was assessed by the Kirby Bauer test. MH agar plates were seeded with $10^8$ CFU/ml of *S. epidermidis* and polymer or $BSA_{np}$-embedded cellulose discs were placed in these Petri plates. Following incubation at 37 °C for 24 h, the diameters of inhibition zones of bacterial growth around the discs were measured. The test was performed on the same disc at 24 h intervals over a period of 10 days.

### 2.2. Sample swelling

The $BSA_{np}$ swelling kinetics was not performed because of nanoparticles aggregation during the drying process and difficulties found in the powder handling for the water uptake experiments. Therefore, BSA nanoparticles with different water contents were obtained firstly by equilibrating nanoparticles in water and secondly by drawing $BSA_{np}$ determined amounts which were then pressed between blotting paper sheets for different time periods. Weighted samples were then sealed in aluminium pan for DSC analysis.

Water uptake kinetics of PEUA and PEUA/$BSA_{np}$ films was followed by immersing the samples in distilled water at room temperature for different time. A portion of the swollen films was punched with a circular die cutter, weighted and sealed in the DSC aluminium pan.

The total water content ($W_{tot}$) was determined after DSC analysis by vacuum drying the samples at 120 °C until a constant weight and calculated as follows:(1)$W_{tot}(wt.\%) = \frac{100\times(w_h - w_0)}{w_0}$ where $w_0$ and $w_h$ are the weights of dry and hydrated sample, respectively.

Protein nanoparticles were designated as $BSA_{np}$ ($W_{tot}$), according to their water content.

### 2.3. Differential scanning calorimetry

Differential scanning calorimetry (DSC) experiments were carried out by using a Mettler DSC821$^e$ apparatus. The phenomena due to water in hydrated materials was analyzed by following the thermal behaviour of the samples in cooling (from 25 to −100 °C) and heating (from −100 to 25 °C) runs at a 5 °C $min^{-1}$ scan rate in $N_2$ atmosphere. The water freezing or melting latent heat values were expressed in Joule per gram of dry sample.

### 2.4. Mechanical and dynamical mechanical tests

To evaluate tensile properties of the dry and hydrated PEUA and PEUA/$BSA_{np}$ samples, stress–strain curves were recorded on 0.02 cm × 1 cm × 5 cm rectangular films by an Instron 4502 test machine, using a 2 KN load-cell and a crosshead speed of 100 mm $min^{-1}$. The strain values were reported as $(L - L_0)/L_0 \times 100$, where $L$ and $L_0$ are the sample lengths after and before the deformation. The Young modulus was determined as the maximum slope of the stress–strain curve.

Dynamic mechanical thermal analysis (DMTA) was carried out in tensile mode by using a Rheometrics Solid Analyzer RSA II. The real ($E'$) and imaginary ($E''$) components of the complex tensile modulus $E^*$ and $\tan\delta = E''/E'$ were investigated by heating the sample at 5 K $min^{-1}$ in the range from −140 °C to 30 °C at a test frequency of 1 Hz and 0.05% dynamic deformation.

## 3. Results and discussion

### 3.1. $BSA_{np}$ characterization

The thermal analysis evidenced that $BSA_{np}$ dry sample did not show any transition in the explored temperature range, while water crystallization and melting processes were observed in the DSC cooling and heating curves of hydrated samples when the water content exceeded a threshold value, as discussed later on. In Fig. 1 the cooling and heating curves of albumin nanoparticles sample containing 370% of water ($BSA_{np}$(370)) are reported.

In the cooling run, the thermogram is characterized by an exothermic peak at −11 °C. In the heating curve, the endothermic melting process starts at about −8 °C (Fig. 1 inset) and results to be composed of several overlapping transitions. The melting behaviour of the swollen samples as a function of water content is reported in Fig. 2 (the heat flow is normalized respect to the dry $BSA_{np}$ weight).

The absence of water transitions below a certain $W_{tot}$ value (29% in Fig. 2) indicates that the freezing water in the samples is less than the one gravimetrically measured and, hence, the presence of a non-freezing water fraction may be inferred.

In addition, Fig. 2 shows that the endothermic peak intensity and shape vary according to the water content.

The $BSA_{np}$(110) thermogram shows a single asymmetric peak at 2 °C with the onset at about −7 °C. By increasing $W_{tot}$, the endothermic process of $BSA_{np}$(305) and $BSA_{np}$(370) samples turns in a structured band characterized by a broad peak at about 4 °C (onset −8 °C) and by a sharp peak at 1 °C. As the water content further increases, the peaks merge into one single broad endothermic process spanning from −10 to 8 °C ($BSA_{np}$(770) and $BSA_{np}$(1030) samples).

Although the DSC analysis cannot efficiently resolve the discrete water states in all the samples, the observed melting behaviour may be ascribed to the evolution of water state distribution at the different $W_{tot}$.

The asymmetric broad peak observed for $110 \le W_{tot} \le 370\%$ is characterized by an onset temperature located well below 0 °C and extends at higher temperature during the relatively high rate dynamic heating. These endothermic processes, as shown later, were associated to the melting of geometrical confined water molecules, while the sharp peaks at 1 °C of $BSA_{np}$(305) and $BSA_{np}$(370) samples, characterized by an extrapolated onset temperature located at about 0 °C, could be attributed to the melting of free water (Capitani et al., 2003). At $W_{tot} \ge 770\%$, the endothermic processes are no more resolved and merge in one broad band.

For a complete picture of water state distribution into the hydrated $BSA_{np}$, the non-freezing water fraction ($W_{nf}$) was evaluated. The total water crystallization ($\Delta H_c$) and melting ($\Delta H_m$)

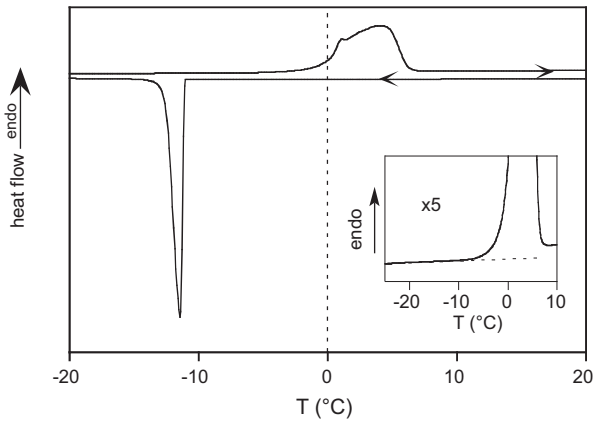


**Fig. 1.** DSC cooling and heating curves of the $BSA_{np}$(370) sample equilibrated in water for 6 h. The inset shows the expanded scale of the melting process onset.

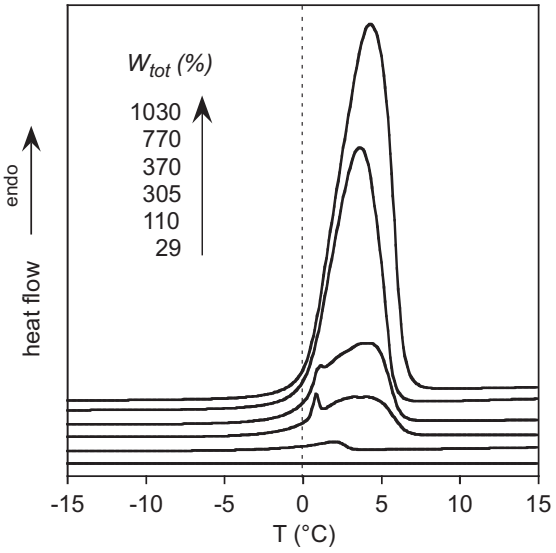


**Fig. 2.** DSC heating curves of $BSA_{np}$ containing different total water contents ($W_{tot}$).

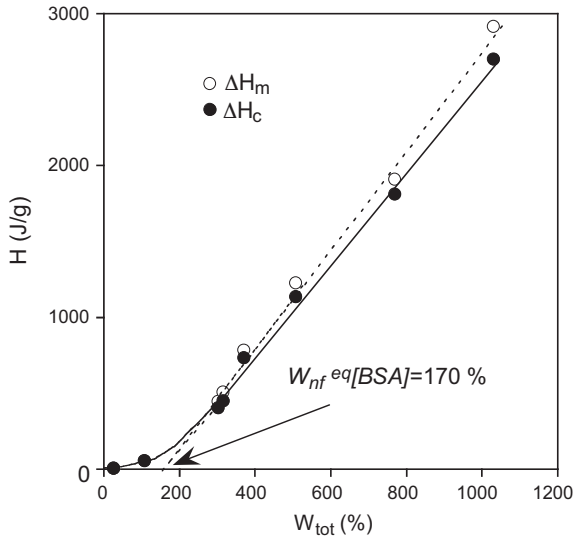


**Fig. 3.** Heat of water crystallization ($\Delta H_c$) and fusion ($\Delta H_m$) measured by DSC as a function of the total water content ($W_{tot}$) in swollen $BSA_{np}$. The lines represent the linear fitting of the melting (dotted line) and crystallization (solid line) data for $W_{tot} > 110\%$. The arrow indicates the equilibrium non-freezing water fraction ($W_{nf}^{eq}$[BSA]) as determined according to the method II (see the text).

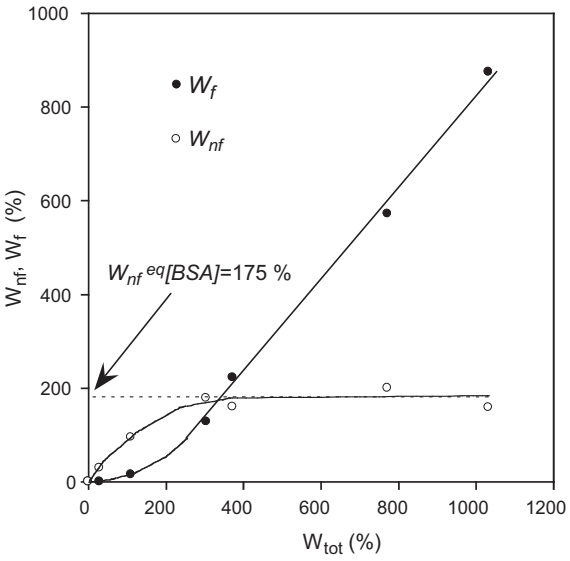


**Fig. 4.** Variation of the non-freezing ($W_{nf}$) and freezing ($W_f$) water fractions as a function of the total water content ($W_{tot}$) in the swollen $BSA_{np}$. The arrow indicates the equilibrium non-freezing water fraction ($W_{nf}^{eq}$[BSA]) as determined according to the method I (see the text).

integrated enthalpy per gram of dry $BSA_{np}$ as a function of the total water content is reported in Fig. 3.

In the hypothesis that the non-freezing water fraction ($W_{nf}$) does not depend on $W_{tot}$, the intercept of the linear regression curve with the *x* axis represents the equilibrium non-freezing water value $W_{nf}^{eq}$[BSA] (method II in Le Dean et al., 2001). The good linear fit obtained by excluding the $BSA_{np}(29)$ and $BSA_{np}(110)$ samples yields a value of $W_{nf}^{eq}[BSA] = 170\%$ for both melting and freezing data sets. The exclusion of the $BSA_{np}(29)$ and $BSA_{np}(110)$ samples, the first two points in Fig. 3, is justified by the fact that when the $W_{tot}$ is below the $W_{nf}^{eq}$[BSA] the independency of $W_{nf}$ on $W_{tot}$ is not verified, probably because of a water molecules redistribution leading to a fraction of non-freezing water into the freezing state.

In alternative, the non-freezing water fraction may be evaluated as the difference between $W_{tot}$ and the total freezing water amount ($W_f$) (method I in Le Dean et al., 2001). By assuming that the heat of fusion of bulk water ($\Delta H_f^w = 333$ J/g) does not depend on the water state or temperature, $W_f$ may be obtained from the ratio between the integrated melting enthalpy and $\Delta H_f^w$ (Le Dean et al., 2001). In Fig. 4 the $W_{nf}$ and $W_f$ values are reported as a function of the total water content.

The $W_{nf}$[BSA] = 175% constant value obtained for $W_{tot} \geq 305\%$ may be considered as the equilibrium non-freezing water fraction determined by the method I. This value is close to that estimated with the method II and supports the approximation about the $\Delta H_f^w$ constancy.

Therefore, the non-freezing ($W_{nf} \times 100/W_{tot}$) and freezing ($[W_{tot} - W_{nf}] \times 100/W_{tot}$) water fractions represent about 57 wt.% and 43% of the total absorbed water, respectively.

Moreover, taking into account the fusion enthalpy value of the $BSA_{np}(305)$ endothermic peak at 1 °C (Fig. 2), determined after deconvolution of the peak related to the freezing water, the amount of free water is about of 2%. Therefore, at $W_{tot} = 305\%$ almost all the freezing water is in a geometrical confined state.

The obtained results have been also confirmed by recent studies on water dynamics and water interaction in $BSA_{np}$ suspension performed on $W_{tot} \sim 300\%$ swollen albumin nanoparticles by analysis of proton NMR relaxation curves and self-diffusion measurements that showed the presence of two well separated relaxation rates (Bellotti et al., 2010). These rates have been accounted for a surface limited relaxation regime of water molecules inside albumin nanoparticles (60 wt.% of the total water content) and a diffusion limited relaxation of water molecules into the meso-cavities between the packed nanoparticles (40 wt.% of the total water content). At higher water content, the appearance of slowly relaxing components was assigned to free water molecules external to the nanoparticles, supernatant on the top of the sample.

Therefore, the non-freezing and freezing water fractions up to $W_{tot} \cong 300\%$, determined by DSC measurements, may be associated to the water molecules inside and between the packed nanoparticles, respectively. While, at higher water content free molecules external to the nanoparticles are also present.

### 3.2. Polyurethane matrix and polyurethane/$BSA_{np}$ composite characterization

To measure the swelling kinetics, about 0.2 mm thick films of PEUA and PEUA/$BSA_{np}$ samples were dwelled in water at room temperature and weighted at different time up to 7 days. The total water content $W_{tot}$ as a function of swelling time is reported in Fig. 5A.

The BSA nanoparticles dispersed in the polyurethane matrix facilitate the water uptake of the composite film, as shown by the faster swelling kinetics and the higher amount of water content shown by PEUA/$BSA_{np}$.

In the absence of data about the $BSA_{np}$ swelling kinetics, the $BSA_{np}$ water uptake $W'_{tot}$[BSA] may be estimated by subtracting the weighted contribution of water in the PEUA to the total PEUA/$BSA_{np}$ water content. In particular, by assuming that the polyurethane matrix swelling is not influenced by the nanoparticles dispersion and by taking into account the composite weight composition (PEUA:BSA = 3:1), $W'_{tot}$[BSA] can be calculated by Eq. (2):

$$W'_{tot}[BSA] = W_{tot}\left[\frac{PEUA}{BSA_{np}}\right] - 0.75 \times W_{tot}[PEUA] \quad (2)$$

The $BSA_{np}$ contribution to the total composite swelling levels off at after about 24 h. Such a value is rather low compared with the potential swelling of the protein nanoparticles alone. In fact, by taking into account only the equilibrium non-freezing water fraction inside the protein particles ($W_{nf}^{eq}[BSA] = 170\%$), $BSA_{np}$ should contribute almost for $W_{tot}[BSA] = 170 \times 0.25 = 42.5\%$.

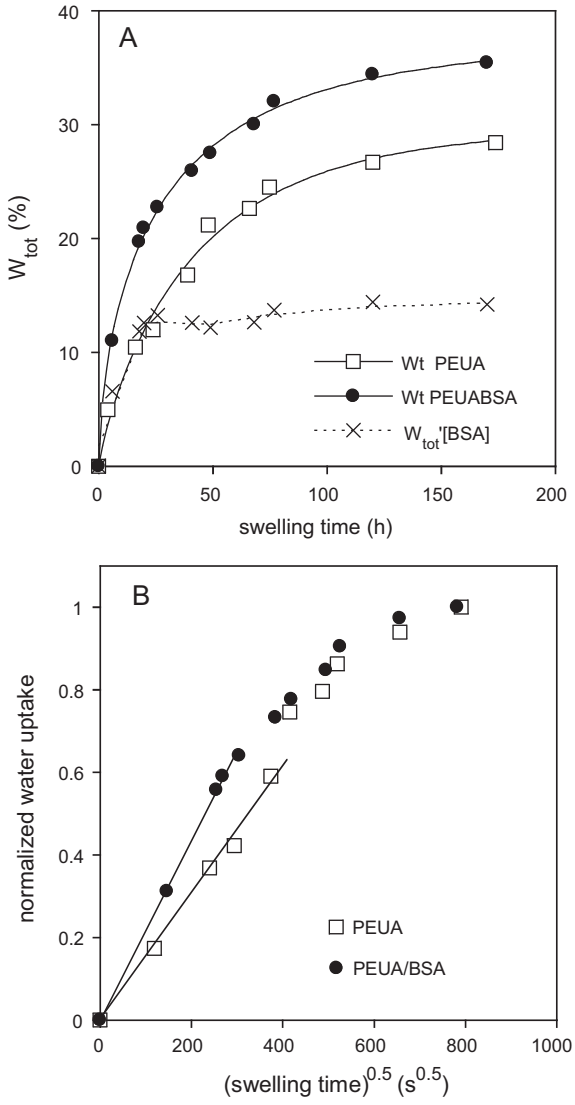


**Fig. 5.** Water swelling kinetics of PEUA and PEUA/$BSA_{np}$ samples (A). $BSA_{np}$ water uptake contribution in the composite was evaluated by Eq. (2). Normalized PEUA and PEUA/$BSA_{np}$ water uptake ($W_{tot}/W_{tot}^{\infty}$) as a function of the square root of the swelling time (B). The diffusion coefficients $D$ were determined from the slopes of the linear part of the plot, according to Eq. (3) (lines represent linear fitting).

The effect of hydrophilic nano-filler on the composite material water uptake is a widely investigated issue depending on a number of parameters, as matrix and filler hydrophilicity, filler concentration and matrix/particles interfacial interactions. In the literature, either higher or lower composite material swelling with respect to the unfilled matrix are reported. In the first case, a direct contribution of hydrophilic filler or the filler/matrix interface on water sorption material capacity is involved (Mamunya et al., 2004; Moon et al., 2001). In the second case, strong interactions between the filler and the matrix may form a rigid three-dimensional network that hampers matrix or interfacial swelling (Kristo and Biliaderis, 2007). Our composite shows an intermediate behaviour, the nanoparticles increased the material swelling but in lower degree than the expected one. As reported later, this may be due to a polyurethane structural change resulting from $BSA_{np}$ incorporation.

From gravimetric water uptake experiments as a function of the swelling time, it is possible to evaluate the water diffusion coefficient $D$ into the samples. In fact, in Fickian diffusion regime, $D$ can be related to the early stage of $W_{tot}$ time evolution according to the approximate equation, usually considered valid for $W_{tot}/W_{tot}^{\infty} \leq 0.6$:

$$\frac{W_{tot}}{W_{tot}^{\infty}} = \frac{4t^{1/2}D^{1/2}}{L\pi^{1/2}} \quad (3)$$

where $W_{tot}^{\infty}$ is the water uptake at equilibrium, $t$ the swelling time and $L$ the film thickness, assumed constant during the absorption process (Pissis et al., 1996). Although the PEUA and PEUA/$BSA_{np}$ films do not reach the hydratation equilibrium in the 170 h explored period, in Eq. (3) the maximum swelling values of $W_{tot}^{\infty}[PEUA] = 28\%$ and $W_{tot}^{\infty}[PEUA/BSA_{np}] = 33\%$ may be used. Fig. 5B shows the normalized water uptake versus the square root of the swelling time. The diffusion coefficients, determined from the initial slope of the straight line interpolating the data, are $D_{PEUA} = (2.2 \pm 0.1) \times 10^{-10}\ cm^2\ s^{-1}$ and $D_{PEUA/BSA_{np}} = (3.4 \pm 0.2) \times 10^{-10}\ cm^2\ s^{-1}$. Actually, the $D_{PEUA/BSA_{np}}$ value is an apparent mean quantity, being determined by the complex combination of water diffusion within the polyurethane matrix, the albumin nanospheres and across their interfaces. It is also interesting to observe that if the protein nanospheres are dried before their dispersion into the polyurethane, particle aggregation occurs. In this case, the composite diffusion coefficient further increases to $3.8 \times 10^{-10}\ cm^2\ s^{-1}$ revealing the high water sorption ability of inter-particles macroscopic voids.

Generally, when highly hydrophilic particles are dispersed in polymer matrices and act as a water trap, a decrease in the diffusion coefficient is observed. A similar $D$ reduction was also observed with the immobilization of penetrating molecules on hydrophilic surface (Garcia de Rodriguez et al., 2006; Lekatou et al., 1997; Sforça et al., 1999). On the contrary, a water $D$ increase was recorded when the nanoparticles favoured the formation of a continuous pathway for the diffusion of water molecules through the composite (Kristo and Biliaderis, 2007).

Although our system is further complicated by the presence of two phases (hard and soft segments) in the polyurethane, we can hypothesize that the diffusion coefficient increase is due to a structural and morphological polyurethane modification induced by $BSA_{np}$ dispersion and involving a higher phase segregation with the formation of regions characterized by different diffusion properties.

A deeper insight into water behaviour within PEUA and PEUA/$BSA_{np}$ films was obtained by following the thermal properties of the swollen samples. In Fig. 6A and B DSC heating profiles of PEUA and PEUA/$BSA_{np}$ at different swelling time are reported.

From the early swelling time, all the samples show a complex water melting behaviour, highlighted by the overlapping of different endothermic processes reflecting the chemical, structural and morphological material heterogeneity. In general, it may be observed a systematic higher value of the transition onset temperature for the composite, revealing an overall higher mean freedom degree of the freezing water molecules into PEUA/$BSA_{np}$. In Fig. 7A and B the total water content ($W_{tot}$) and the freezing ($W_f$) and non-freezing ($W_{nf}$) fractions, calculated according to the previously described method I, are reported as a function of the swelling time.

The values of the non-freezing water amount at plateau (method I) $W_{nf}^{eq}[PEUA] = 11\%$ and $W_{nf}^{eq}[PEUA/BSA_{np}] = 19\%$ are in good agreement with the results derived by using method II ($W_{nf}^{eq}[PEUA] = 10\%$, $W_{nf}^{eq}[PEUA/BSA_{np}] = 18\%$), reported in Fig. 8.

Fig. 7A and B clearly show the effect of albumin nanoparticles dispersed in PEUA on the water distribution within the samples. First, it may be observed that the higher $W_{tot}[PEUA/BSA_{np}]$ value is essentially due to the rapid increase of the non-freezing water fraction (a 58% value with respect to the maximum swelling value of the composite at about 24 h), indicating that the water molecules are readily absorbed to the protein nano-spheres by strong inter-

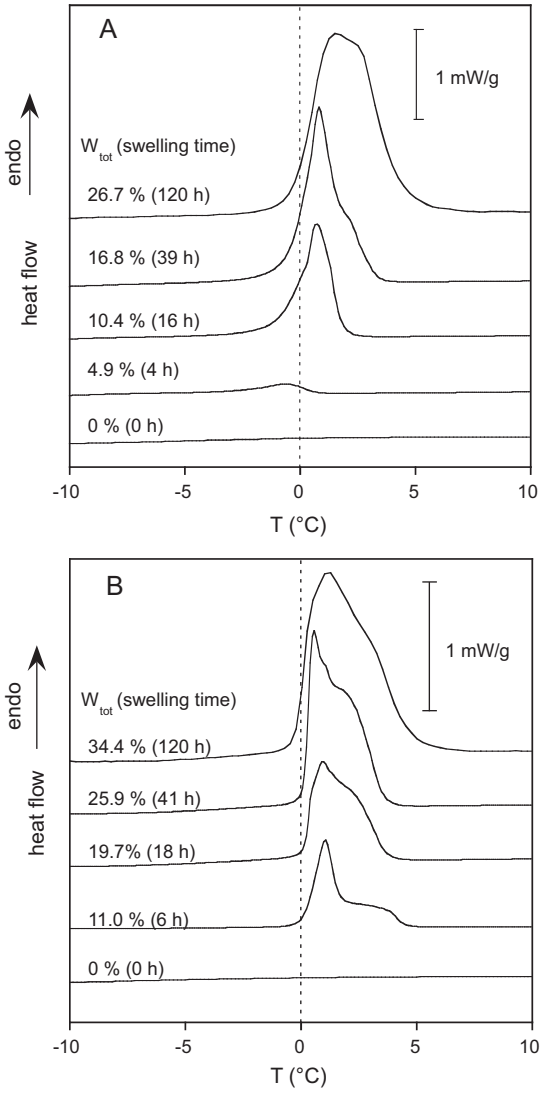


**Fig. 6.** Representative DSC heating curves of dry and swollen PEUA (A) and PEUA/$BSA_{np}$ (B) samples.

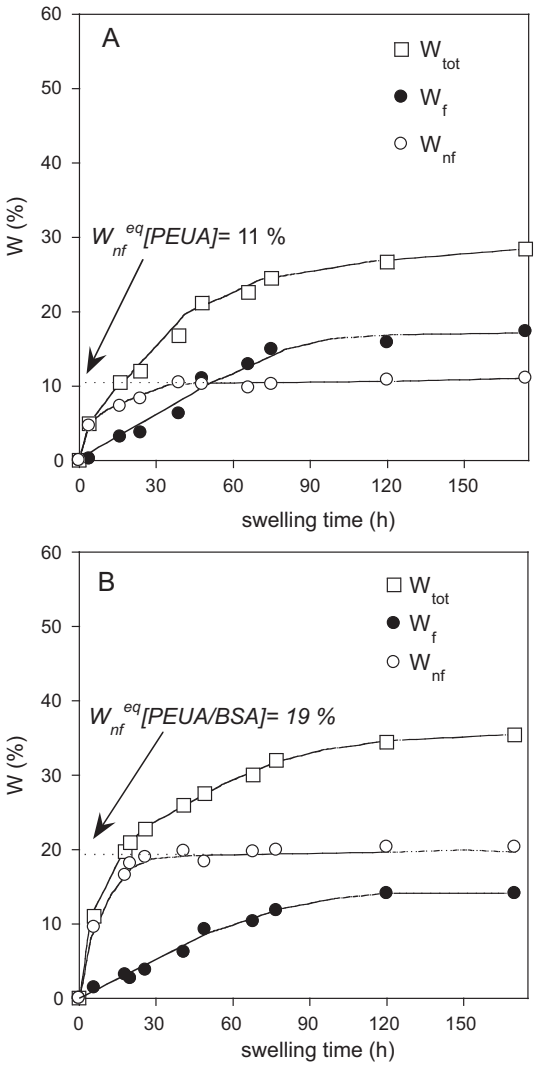


**Fig. 7.** Total water content ($W_{tot}$) and the freezing ($W_f$) and non-freezing ($W_{nf}$) fractions in PEUA (A) and PEUA/$BSA_{np}$ (B) samples as a function of the swelling time. The arrows indicate the equilibrium non-freezing water fraction as determined according to the method I.

actions. Indeed, after the normalization with respect to the sample composition, it can be noted that the $BSA_{np}$ addition into PEUA enhances the $W_{nf}$[PEUA/$BSA_{np}$] value but does not greatly affect the kinetics nor the equilibrium value of the freezing water uptake in the polyurethane (at a swelling time of 174 h, the normalized PEUA freezing water fraction is $W_f$[PEUA] × 0.75 = 13% while for the composite $W_f$[PEAU/$BSA_{np}$] = 14%).

The obtained results can be exploited to understand the composite material behaviour toward drug uptake and release. BSA nanoparticles were able to load 0.2 ± 0.1 mg of cefamandole nafate (CEF) per mg of nanoparticles and to release the drug by two different release kinetics: a rather rapid elution in the first 5 h (about 68% cumulative release, Fig. 9A) followed by a slower one in the next 48 h, reaching a 75% plateau value (data not shown). For such system a moderate bacterial activity up to 4 days was observed (Fig. 9B).

According to DSC data, it may be inferred that the rapid drug release is due to the freezing water fraction present on the surface and between the packed BSA nanoparticles. Indeed, since the drug adsorption experiments were carried out keeping $BSA_{np}$ in antibiotic solution for 24 h, it can be hypothesized that nanoparticles were in a completely hydrated state and that the contribution of the freezing water fraction to the total swelling was higher than the non-freezing one. This is supported by the data reported in Fig. 4 that evidence as only for low swelling the $W_f$ value is lower than that of $W_{nf}$ fraction. Therefore, the initial burst release is due to a swelling-dependent mechanism followed by a slower diffusion-dependent one related to the non-freezing water fraction.

As for PEUA alone, the polymer loaded a low antibiotic amount (0.027 ± 0.003 mg CEF per mg of PEUA) and showed inhibition zones of bacterial growth only for few hours owing to the low released drug amount, corresponding to about $5 \times 10^{-3}$ mg of the antibiotic released in the first hour (Fig. 9A).

This is likely due to the poor water swelling of the polymer that hinders the diffusion of the drug from the bulk to the surface (diffusion barrier).

When the nanoparticles were entrapped in the polyurethane matrix, the composite showed a higher drug loading with respect to PEUA (0.10 ± 0.01 mg of CEF per mg of composite) but a slower drug release. Indeed, although the release percentage at 2 h elution is similar for PEUA and the composite (Fig. 9A), this latter keeps releasing cefamandole in active concentrations up to 9 days, as evidenced by Kirby Bauer test (Fig. 9B).

The higher drug loading observed for the composite with respect to PEUA alone may be due both to the greater PEUA hard/soft phase

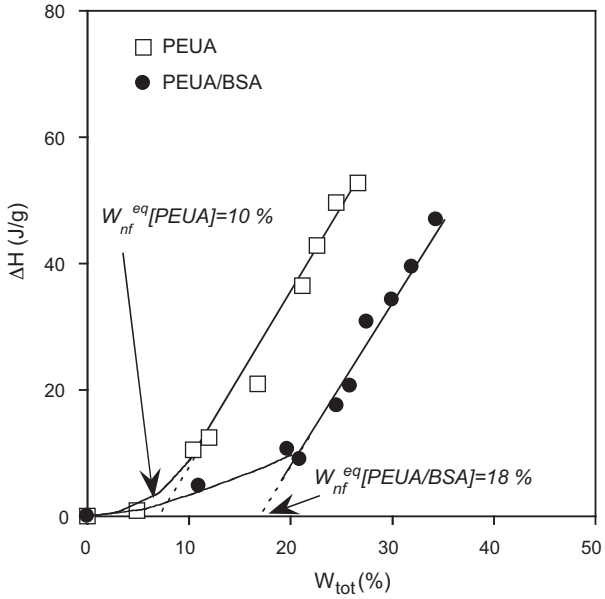


**Fig. 8.** Water heat of fusion ($\Delta H_m$) measured by DSC as a function of the total water content ($W_{tot}$) in swollen PEUA and PEUA/$BSA_{np}$. The lines represent the linear fitting of the melting data and the arrow the equilibrium non-freezing water fraction ($W_{nf}^{eq}$[PEUA] and $W_{nf}^{eq}$[PEUA/$BSA_{np}$]) as determined according to the method II.

segregation (caused by strong interactions established between the polymer matrix and the dispersed BSA particles that improved drug-matrix affinity) and to the enhancement of the $W_{nf}$ water fraction that allows the diffusion of the drug within the BSA nanoparticles.

It is worth noticing that, at 24 h composite swelling, the introduction of BSA nanoparticles in PEUA only increased the non freezing water fraction but not the freezing one. This peculiar finding allows PEUA/$BSA_{np}$ sample to better control drug release by a diffusion based mechanism, avoiding an initial burst delivery, differently from what observed in $BSA_{np}$ for which the freezing water fraction was high.

In conclusion, in a drug delivery system a greater freezing water fraction may be accountable for a rapid drug release (burst effect), due to a swelling dependent mechanism, while a higher non-freezing fraction brings about to a slower drug elution owing to a diffusion dependent mechanism (a more controlled release). In our case, a better control of drug release was obtained also by the contribution of the dual diffusion barrier consisting of the matrix and nanoparticles along with the tight interactions established between CEF molecules and BSA nanoparticles prolonging the antibacterial activity of the system up to 9 days

To verify the set up of strong interactions between the protein nanoparticles and the polyurethane, thermal and mechanical properties of PEUA and PEUA/$BSA_{np}$ samples were studied and compared. It has already been observed that the carboxylated polyurethanes show poor phase segregation and, hence, high soft segment $T_g$ and partially viscous mechanical behaviour. This is due to the interaction between the proton of the carboxylic group in the hard segment and the oxygen atom of the soft segment and to an easier intercalation of the soft chains into the hard segments due to steric hindrance of bulky dihydroxymethyl-propionic acid (Čulin et al., 2004). The addition of BSA nanoparticles decreased the PEUA $T_g$ from −3 °C to −9 °C so evidencing a partial phase separation of the polyurethane matrix, induced by the interactions of the polymer hard segments with the protein particle surface (Table 1).

The change in the polyurethane structure upon $BSA_{np}$ dispersion, beside the water uptake and diffusion behaviour, has a

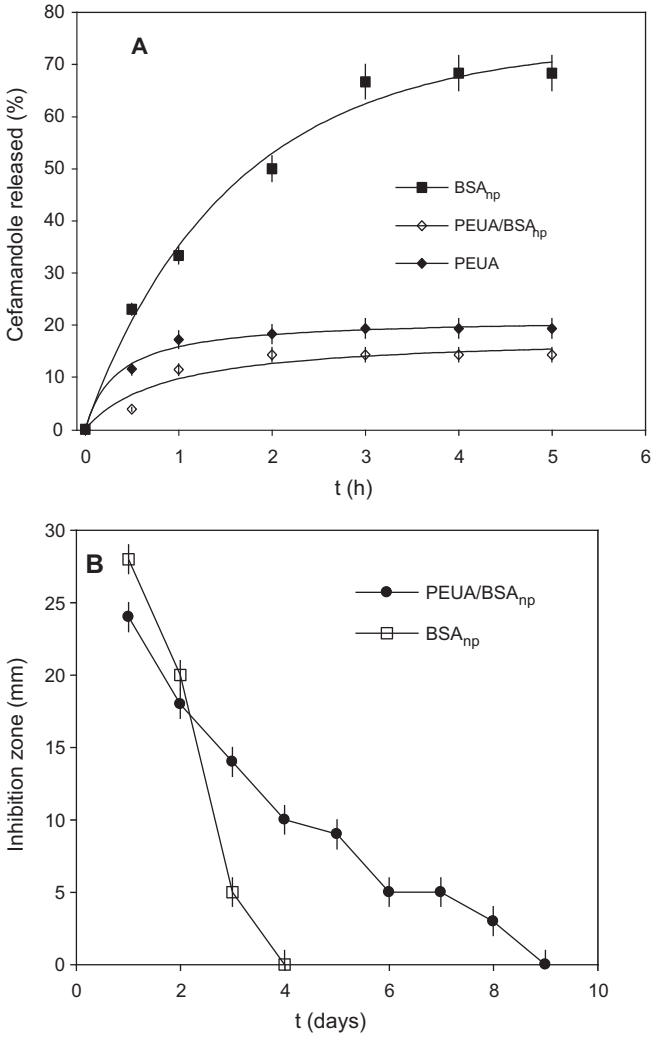


**Fig. 9.** Cefamandole release from $BSA_{np}$, PEUA and PEUA/$BSA_{np}$ (A). Inhibition zone of *S. epidermidis* growth measured around composite and $BSA_{np}$-embedded cellulose discs (B).

direct influence on the composite mechanical properties. In fact, the nanoparticles act as an effective reinforcing filler increasing the Young modulus from 1.4 MPa for PEUA to 44 MPa for PEUA/$BSA_{np}$ and decreasing the viscous flow after the yielding point. In Fig. 10 the stress–strain curves of dry and 48 h swollen PEUA and PEUA/BSA samples are reported.

The dry PEUA and PEUA/$BSA_{np}$ mechanical profiles were taken for sake of comparison from Crisante et al. (2009). It is well known that the absorbed water has a plasticization effect on the segmented polyurethane, decreasing its $T_g$ and stiffness (Pissis et al., 1996). After the water swelling, the hydrated composite, preserves good mechanical properties, the Young modulus and tensile

**Table 1**
Thermal, mechanical and dynamic mechanical properties of dry and 48 h swollen PEUA and PEUA/BSA.

| Sample | Young modulus, MPa | Tensile strength, MPa | $T_g$, °C[a] | $T_\alpha$, °C[b] |
|---|---|---|---|---|
| PEUA | 1.4 | 0.35 | −3 | 9 |
| PEUA/BSA | 44 | 2.1 | −9 | 3 |
| PEUA (48 h swollen) | 0.4 | 0.07 | −17 | −5 |
| PEUA/BSA (48 h swollen) | 9.0 | 0.8 | −19 | −1 |

[a] DSC data.
[b] DMTA data.

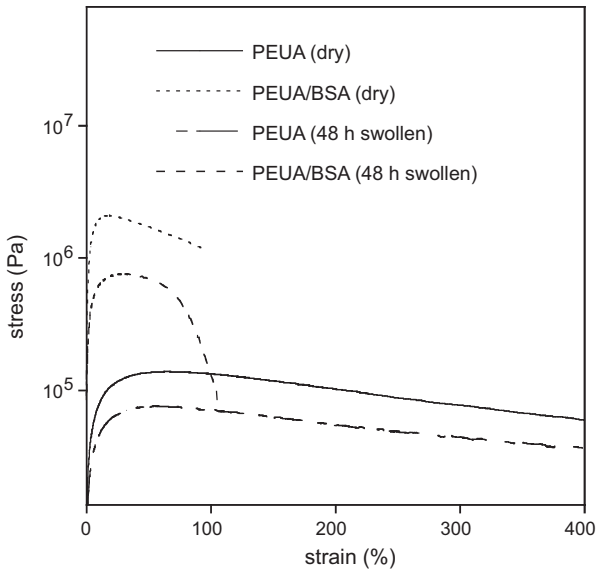


**Fig. 10.** Stress–strain curves of dry and 48 h swollen samples.

strength remaining higher than those of dry PEUA (Table 1). Similar behaviour was observed in waterborne polyurethane/casein composites by Wang et al. (2004), who reported a $T_g$ decrease and a tensile strength increase as higher was the protein amount into the sample. The authors also observed that the swollen samples showed enhanced mechanical properties.

The dynamic mechanical properties of the dry and 48 h swollen PEUA ($W_{tot}$ = 21%) and PEUA/$BSA_{np}$ ($W_{tot}$ = 27%) samples are shown in Fig. 11A and B, where the temperature dependence of the storage modulus $E'$ and of the loss factor tan $\delta$ are reported.

The PEUA stiffness increase due to the $BSA_{np}$ dispersion was confirmed also in the DMTA tests. As shown in Fig. 11A, PEUA/$BSA_{np}$ nano-composite exhibits higher $E'$ in all the explored temperature range. Moreover, PEUA α relaxation at $T_\alpha^{PEUA} = 9\,^\circ C$, associated to the soft segment glass transition, is characterized by the drastic $E'$ modulus drop typical of a poorly segregated polyurethane (Yang and Lin, 2001). On the other hand, PEUA/$BSA_{np}$ sample shows the usual composite behaviour, in which the interacting rigid phase ($BSA_{np}$) partially prevents the large creeping due to the glass transition at $T_\alpha^{PEUA/BSA_{np}} = 3\,^\circ C$. At lower temperature, the two other relaxations, β and γ, at about $T_\beta = -90\,^\circ C$ and $T_\gamma = -130\,^\circ C$ are typical of segmented polyurethane as well as other hydrogen bond forming polymers, as polyamides (Jacobs and Jenckel, 1961; Laredo et al., 2003). The β transition was attributed to the water molecules interacting by hydrogen bond with the hard segment polar groups. It disappears only after a complete sample drying and readily regains its original intensity by exposing the polymer to atmospheric moisture. The γ mode is related to the local motion of the soft segment chains.

The swelling brings about to a variation in the sample dynamic mechanical behaviour, especially in correspondence of PEUA α relaxation (Fig. 11B). At lower temperature the β peak intensity increases, especially in PEUA/$BSA_{np}$ sample, confirming the influence of the absorbed water on such a relaxation.

The well known water plasticization effect on polyurethane glass transition, already observed by DSC analysis (Table 1), is evidenced by $T_\alpha^{PEUA/BSA_{np}}$ shift at lower temperature (Table 1). The offset is associated with a small broadening of the peak. On the other hand, the PEUA α relaxation undergoes a large shape change. In fact, after the water uptake, the transition results to be composed by two broad overlapped peaks at $-5\,^\circ C$ and $4\,^\circ C$ and a hump at $-30\,^\circ C$. Such behaviour reflects the effect of the different interactions that the absorbed water can establish with the complex phase mixed/segregated PEUA structure. The water molecules, which can easily diffuse into the polymer domains characterized by a minor cohesion, weaken the interactions between the mixed hard and soft phase and favour the segmental mobility of polyether, which relaxes at lower temperature. The uneven water distribution into the polymer is also enlightened by the presence of the higher temperature α relaxation peak which does not largely changes its position with respect to the dry sample. The detailed phenomena interpretation needs further investigation. However, analogous phenomena were also observed when the carboxylated polyurethane was exposed to the vapour of other hydrogen bond forming liquids, like ethylic ether or ethanol (data not reported) (Pacella, 1999).

The higher PEUA/$BSA_{np}$ phase segregation, induced by the preferential interaction of the hard segment with the $BSA_{np}$ surface, gives rise to a more homogeneous water distribution into the partially segregated soft phase, which relaxes on the whole at lower temperature. This improved phase segregation also explains the increase of the composite diffusion coefficient previously observed in water uptake experiments.

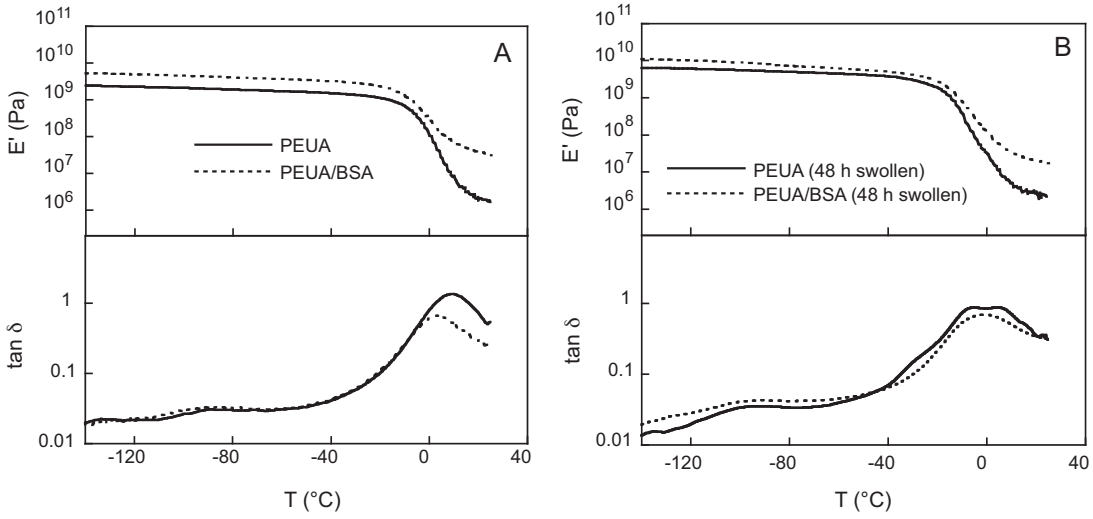


**Fig. 11.** Elastic modulus ($E'$) and loss factor (tan $\delta$) of the of dry (A) and 48 h swollen (B) samples vs. temperature.

In conclusion, in the preparation of nanostructured composites employable for drug controlled delivery devices, the two requirements of tight interactions between the system components (i.e. drug/nanoparticles/polymer matrix) and a high non freezing water fraction adsorbed to the system itself need to be fulfilled. In this way, a higher drug adsorption along with a controlled drug release as well as an improvement in material stiffness can be obtained allowing the development of a system suitable for the manufacturing of different types of medical devices including intravascular catheters.

## 4. Conclusions

Whereas a single material cannot fulfil the complex task required for a particular application, the mixing of more components may represent a valid strategy to overcome the problem. Moreover, the presence of a synergistic effect among the mixture components represents the best opportunity in composite material preparation. A successful example of such strategy has been recently proposed by our group for the development of an antibiotic controlled release system to be employed for the prevention of medical device-related infections. The antibiotic-loaded system consisted of a carboxylated polyurethane (PEUA) containing bovine serum albumin nanoparticles ($BSA_{np}$) which act as drug reservoir. In order to better understand the PEUA/$BSA_{np}$ composite drug release properties and the mechanical behaviour, a detailed physical investigation on the material and on its interaction with absorbed water was carried out.

By comparing the $BSA_{np}$, PEUA and PEUA/$BSA_{np}$ total water uptake and the water distribution into the samples, determined by DSC experiments, it was possible to assess that, in $BSA_{np}$ sample, the water can adsorb both in the inter-particles regions and inside the particles. The inside nanoparticle fraction is in a non-freezing state because of the strong interaction between the water molecules and the protein polar groups. With increasing of total adsorbed water amount, the contribution of the freezing water fraction to the swelling was higher than the non-freezing one. As for PEUA, the majority of water molecules absorbed is in a mobile freezing state (about 60% of the $W_{tot}$).

The PEUA/$BSA_{np}$ composite swells more than PEUA, but the experimental swelling value is less than that expected by taking into account the water uptake contribution of the single components. Moreover, the higher PEUA/$BSA_{np}$ swelling is due to the non-freezing water fraction increase, caused by the nanoparticles dispersion. The enhancement of non-freezing water fraction lets the composite not only to increase the drug loading but also to control its release through tight interactions between CEF molecules and BSA nanoparticles. These interactions along with the dual diffusion barrier consisting of the matrix and nanoparticles prolonged the antibacterial activity of the system up to 9 days.

The higher drug loading of the composite with respect to PEUA may be also due to the greater polymer hard/soft phase segregation (caused by strong interactions established between the polymer matrix and the dispersed BSA particles that improved drug-matrix affinity) as evidenced by thermal and mechanical analysis.

In conclusion, differently from the single components the developed nanostructured composite was able to control cefamandole release for long term and possessed good mechanical properties. Therefore, we can hypothesize that this system possesses the suitable features for the manufacturing of different types of antimicrobial medical devices, including intravascular catheter. Further studies are necessary to verify the in vivo efficacy of the formulation herein proposed, which may be tuned by varying, for example, the nanoparticles size or the loaded drug (other antibiotic kind, antiseptic or antifungal agents).

## Acknowledgements

The authors wish to thank *University and Research Italian Ministry* (MIUR) for financial support.

## References

Aoki, S., Ando, H., Ishii, M., Watanabe, S., Ozawa, H., 1995. Water behavior during drug release from a matrix as observed using differential scanning calorimetry. J. Control. Release 33, 365–374.

Akasaka, Y., Ueda, H., Takayama, K., Machida, Y., Nagai, T., 1988. Preparation and evaluation of bovine serum albumin nanospheres coated with monoclonal antibodies. Drug Des. Deliv. 3, 85–97.

Bellotti, M., Martinelli, A., Gianferri, R., Brosio, E., 2010. A proton NMR relaxation study of water dynamics in bovine serum albumin nanoparticles. Phys. Chem. Chem. Phys. 12, 516–522.

Capitani, D., Mensitieri, G., Porro, F., Proietti, N., Segre, A.L., 2003. NMR and calorimetric investigation of water in a superabsorbing crosslinked network based on cellulose derivatives. Polymer 44, 6589–6598.

Crisante, F., Francolini, I., Bellusci, M., D'Ilario, L., Martinelli, A., Piozzi, A., 2009. Antibiotic delivery polyurethanes containing albumin and polyallylamine nanoparticles. Eur. J. Pharm. Sci. 36, 555–564.

Čulin, J., Andreis, M., Šmit, I., Veksli, Z., Anžlovar, A., Žigon, M., 2004. Motional heterogeneity and phase separation of functionalized polyester polyurethanes. Eur. Polym. J. 40, 1857–1866.

D'Ilario, L., Martinelli, A., Piozzi, A., Volponi, V., 2002. Mark-Houwink-Sakurada constants for carboxylated segmented polyurethane. J. Macromol. Sci. Phys. 41, 615–628.

Elomaa, M., Hietala, S., Paronen, M., Walsby, N., Jokela, K., Serimaa, R., Torkkeli, M., Lehtinen, T., Sundholm, G., Sundholm, F., 2000. The state of water and the nature of ion clusters in crosslinked proton conducting membranes of styrene grafted and sulfonated poly(vinylidene fluoride). J. Mater. Chem. 10, 2678–2684.

Faroongsang, D., Sukonrat, P., 2008. Thermal behavior of water in the selected starch- and cellulose-based polymeric hydrogels. Int. J. Pharm. 352, 152–158.

Francolini, I., Ruggeri, V., Martinelli, A., D'Ilario, L., Piozzi, A., 2006. Novel metal-polyurethane complexes with enhanced antimicrobial activity. Macromol. Rapid Commun. 27, 233–237.

Francolini, I., D'Ilario, L., Guaglianone, E., Donelli, G., Martinelli, A., Piozzi, A., 2010. Polyurethane anionomers containing metal ions with antimicrobial properties: Thermal, mechanical and biological characterization. Acta Biomater. 6, 3482–3490.

Garcia de Rodriguez, N.L., Thielemans, W., Dufresne, A., 2006. Sisal cellulose whiskers reinforced polyvinyl acetate nanocomposites. Cellulose 13, 261–270.

Green, M.R., Manikhas, G.M., Orlov, S., Afanasyev, B., Makhson, A.M., Bhar, P., Hawkins, M.J., 2006. Abraxane®, a novel Cremophor®-free, albumin-bound particle form of paclitaxel for the treatment of advanced non-small-cell lung cancer. Ann. Oncol. 17, 1263–1268.

Hanaki, K-i., Moto, A., Oku, T., Komoto, A., Maenosono, S., Yamaguchi, Y., Yamamoto, K., 2003. Semiconductor quantum dot/albumin complex is a long-life and highly photostable endosome marker. Biochem. Biophys. Res. Commun. 302, 496–501.

Hatakeyama, H., Hatakeyama, T., Thermochim, 1998. Interaction between water and hydrophilic polymers. Thermochim. Acta 308, 3–22.

Hirata, Y., Miura, Y., Nakagawa, T., 1999. Oxygen permeability and the state of water in Nafion® membranes with alkali metal and amino sugar counterions. J. Membr. Sci. 163, 357–366.

Jacobs, H., Jenckel, E., 1961. Dynamisch-mechanische eigenschaften von polyurethan. 2. Mitt. Der einfluß von quellungsmitteln auf das mechanische verhalten von polyurethane. Makromol. Chem. 47, 72–85.

Katzhendler, I., Mader, K., Friedman, M., 2000. Structure and hydration properties of hydroxypropyl methylcellulose matrices containing naproxen and naproxen sodium. Int. J. Pharm. 200, 161–179.

Kristo, E., Biliaderis, C.G., 2007. Physical properties of starch nanocrystal-reinforced pullulan films. Carbohydr. Polym. 68, 146–158.

Laredo, E., Grimau, M., Sánchez, F., Bello, A., 2003. Water absorption effect on the dynamic properties of nylon-6 by dielectric spectroscopy. Macromolecules 36, 9836–9839.

Le Dean, A., Mariette, F., Lucas, T., Marin, M., 2001. Assessment of the State of Water in Reconstituted Milk Protein Dispersions by Nuclear Magnetic Resonance (NMR) and Differential Scanning Calorimetry (DSC). LWT Food Sci. Technol. 34, 299–305.

Lekatou, A., Faidi, S.E., Ghidaoui, D., Lyon, S.B., Newman, R.C., 1997. Effect of water and its activity on transport properties of glass/epoxy particulate composites. Composites A: Appl. Sci. 28, 223–236.

Li, W., Xue, F., Cheng, R., 2005. States of water in partially swollen poly(vinyl alcohol) hydrogels. Polymer 46, 12026–12031.

Luukkonen, P., Maloney, T., Rantanen, J., Paulapuro, H., Yliruusi, J., 2001. Microcrystalline cellulose-water interaction—a novel approach using thermoporosimetry. Pharm. Res. 18, 1562–1569.

Mamunya, Y.P., Shtompel, V.I., Lebedev, E., Pissis, P., Kanapitsas, A., Boiteux, G., 2004. Structure and water sorption of polyurethane nanocomposites based on organic and inorganic components. Eur. Polym. J. 40, 2323–2331.

Marconi, W., Martinelli, A., Piozzi, A., Zane, D., 1992. Synthesis and physicochemical characterization of a hydrophilic polyurethane able to bind heparin. Biomaterials 13, 432–564.

Marconi, W., Barontini, P., Martinelli, A., Piozzi, A., 1993. New polyurethane compositions containing high amounts of covalently bonded heparin. Makromol. Chem. 194, 347–356.
Marconi, W., Martinelli, A., Piozzi, A., Zane, D., 1991. Direct synthesis of carboxylated polyurethanes. Eur. Polym. J. 27, 135–139.
Merodio, M., Arnedo, A., Renedo, M.J., Irache, J.M., 2001. Ganciclovir-loaded albumin nanoparticles: characterization and in vitro release properties. Eur. J. Pharm. Sci. 12, 251–259.
Michaelis, K., Hoffmann, M.M., Dreis, S., Herbert, E., Alyautdin, R.N., Michaelis, M., Kreuter, J., Langer, K., 2006. Covalent linkage of apolipoprotein E to albumin nanoparticles strongly enhances drug transport into the brain. J. Pharmacol. Exp. Ther. 317, 1246–1253.
Moon, H.T., Lee, J.-K., Han, J.K., Byun, Y., 2001. A novel formulation for controlled release of heparin–DOCA conjugate dispersed as nanoparticles in polyurethane film. Biomaterials 22, 281–289.
Pacella, C., 1999. Caratterizzazione dinamo meccanica di un poliuretano carbossilato. Master Thesis, Sapienza University of Rome, Rome, Italy, October.
Ping, Z.H., Nguyen, Q.T., Chen, S.M., Zhou, J.Q., Ding, Y.D., 2001. States of water in different hydrophilic polymers – DSC and FTIR studies. Polymer 42, 8461–8467.
Piozzi, A., Francolini, I., Occhiaperti, L., Venditti, M., Marconi, W., 2004a. Antimicrobial activity of polyurethanes coated with antibiotics: a new approach to the realization of medical devices exempt from microbial colonization. Int. J. Pharm. 280, 173–183.
Piozzi, A., Francolini, I., Occhiaperti, L., Di Rosa, R., Ruggeri, V., Donelli, G., 2004b. Polyurethanes loaded with antibiotics: influence of polymer-antibiotic interactions on in vitro activity against *Staphylococcus epidermidis*. J. Chemother. 16, 66–69.
Pissis, P., Apekis, L., Christodoulides, C., Niaounakis, M., Kyritsis, A., Nedbal, J., 1996. Water effects in polyurethane block copolymers. J. Polym. Sci. B: Polym. Phys. 34, 1529–1539.
Rault, J., Gref, R., Ping, Z.H., Nguyen, Q.T., Néel, J., 1995. Glass transition temperature regulation effect in a poly(vinyl alcohol)—water system. Polymer 36, 1655–1661.
Ruggeri, V., Francolini, I., Donelli, G., Piozzi, A., 2007. Synthesis, characterisation and in vitro activity of antibiotic releasing polyurethanes able to prevent bacterial resistance. J. Biomater. Mater. Res. A 81, 287–298.
Schneider, N.S., Illinger, J.L., Karasz, F.E., 1993. Effect of water on the glass transition temperature of hydrophilic polyurethanes. J. Appl. Polym. Sci. 48, 1723–1729.
Sforça, M.L., Yoshida, I.V.P., Nunes, S.P., 1999. Volume organic–inorganic membranes prepared from polyether diamine and epoxy silane. J. Membr. Sci. 159, 197–207.
Siepmann, J., Peppas, N.A., 2001. Modeling of drug release from delivery systems based on hydroxypropyl methylcellulose (HPMC). Adv. Drug Deliv. Rev. 48, 139–157.
Tanaka, M., Mochizuki, A., Ishii, N., Motomura, T., Hatakeyama, T., 2002. Study of blood compatibility with poly(2-methoxyethyl acrylate). Relationship between water structure and platelet compatibility in poly(2-methoxyethylacrylate-co-2-hydroxyethylmethacrylate). Biomacromolecules 3, 36–41.
Tanaka, M., Mochizuki, A., 2004. Effect of water structure on blood compatibility-thermal analysis of water in poly(meth)acrylate. J. Biomed. Mater. Res. 68A, 684–695.
Wang, N., Zhang, L., Lu, Y., 2004. Effect of the particle size in dispersions on the properties of waterborne polyurethane/casein composites. Ind. Eng. Chem. Res. 43, 3336–3342.
Weber, C., Coester, C., Kreuter, J., Langer, K., 2000. Desolvation process and surface characterisation of protein nanoparticles. Int. J. Pharm. 194, 91–102.
Yang, J.M., Lin, H.T., 2001. Wettability and protein adsorption on HTPB-based polyurethane films. J. Membr. Sci. 187, 159–169.
Zentner, G.M., Cardinal, J.R., Feijen, J., Song, S.-Z., 1979. Progestin permeation through polymer membranes IV: mechanism of steroid permeation and functional group contributions to diffusion through hydrogel films. J. Pharm. Sci. 68, 970–975.